



Density limit studies on DIII-D

R. Maingi^{b,*}, M.A. Mahdavi^a, T.W. Petrie^a, L.R. Baylor^b, T.C. Jernigan^b,
R.J. La Haye^a, A.W. Hyatt^a, M.R. Wade^b, J.G. Watkins^c, D.G. Whyte^d

^a General Atomics, P.O. Box 85608, MS 13-464, San Diego, CA 92186-5608, USA

^b Oak Ridge National Laboratory, Oak Ridge, TN, USA

^c Sandia National Laboratories, Albuquerque, NM, USA

^d University of California, San Diego, CA, USA

Abstract

We have studied the processes limiting plasma density and successfully achieved discharges with density $\sim 50\%$ above the empirical Greenwald scaling with H-mode energy confinement. This was accomplished by density profile control, enabled through pellet injection and divertor pumping. Several density-limiting mechanisms, including MARFEs and pellet loss processes, were successfully avoided. Finally we have looked in detail at the first and most common density limit process in DIII-D, total divertor detachment, and found that the local upstream separatrix density ($n_e^{\text{sep,det}}$) at detachment onset (partial detachment) increases with the scrape-off layer heating power, P_{heat} , i.e. $n_e^{\text{sep,det}} \sim P_{\text{heat}}^{0.8}$. This is in marked contrast to the line-average density at detachment which is insensitive to the heating power. Our data are in reasonable agreement with the Borass model, which predicted that the upstream density at detachment would increase as $P_{\text{heat}}^{0.7}$. © 1999 Elsevier Science B.V. All rights reserved.

Keywords: Density limits; Divertor detachment; MARFE; Pellet fueling; Divertor pumping

1. Introduction

There is a large tokamak data base supporting a density limit that scales only as $I_p/\pi a^2$, where I_p is plasma current and a is minor radius. This limit is independent of the toroidal field (B_t), heating power (P_{heat}), and other shape and size parameters and is known [1] as the Greenwald limit (n_{GW}). Based on gas-fueled Alcator-C discharges, Greenwald postulated the limit was caused by the reduction in gas/divertor fueling efficiency at high density. With sufficient central fueling from pellets, the density was increased in Alcator-C discharges, although at the cost of a rapid decrease in particle confinement time. This same density limit scaling has been shown to apply to the disruptive limit in ohmic and L-mode plasmas. In L-mode, plasma termination at the density limit is frequently correlated with growth of low m , n magnetohydrodynamic (MHD)

modes and disruption. In H-mode a different behavior has been observed [2] in D-III and DIII-D discharges. Gas fueling at densities $\gtrsim 0.8 n_{\text{GW}}$ resulted in confinement deterioration and transition to L-mode without a significant increase in the line average density, \bar{n}_e .

Greenwald scaling has presented a challenge to the plasma physics community because theories predict additional dependencies, e.g. heating power (P_{heat}) and impurity concentration (n_z/n_e). The scaling has consequences for fusion reactors: many D-T reactor designs must operate above this limit to approach economic competitiveness with other energy production technologies. Theories indicate that several distinct processes exist which can limit density in either the core, edge, or divertor plasma. Motivated by ITER's need [3] to operate at $\bar{n}_e > n_{\text{GW}}$ with H-mode energy confinement, a multi-year experimental campaign has been carried out in DIII-D to investigate these density-limiting processes. These processes include partial divertor detachment (which can lead to divertor collapse), particle confinement and fueling limits, MARFE formation, and MHD activity. These processes and the circumvention

* Corresponding author. Tel.: +1 619 455 4420; fax: +1 619 455 3569; e-mail: maingi@gav.gat.com

techniques are discussed below. Since partial divertor detachment can lead to the most common density limiting process, i.e. total detachment and core MARFE formation, a dedicated experiment to measure local edge plasma parameters at partial detachment onset as a function of heating power is discussed in Section 2. Comparisons with a scrape-off layer (SOL) plasma transport model are presented in Section 3.

Now we briefly discuss the various density limiting processes listed above, starting with partial detachment; Ref. [4] has more details. When the divertor electron temperature (T_e) reaches a few eV, partial divertor detachment (PDD) is observed and the plasma pressure and ion current near the divertor strike point drop in both L-mode and H-mode plasmas. If the \bar{n}_e is increased further, the divertor T_e drops and the divertor radiation increases resulting in thermal collapse. This is followed by effective impurity penetration into the core plasma, a sudden reduction of edge temperature, and shrinkage of the current channel and/or the formation of an X-point MARFE. Experimentally, energy confinement is reduced from H-mode to L-mode levels if the density is increased ≥ 10 –30% after the onset of partial detachment. We bypassed divertor collapse as a density limiting process by maintaining the SOL electron density (n_e) below the divertor collapse limit with divertor pumping, and increasing [4] the ratio of \bar{n}_e to SOL n_e with pellet fueling. Several particle confinement and fueling limits were observed but these could be overcome with proper discharge tailoring. MARFE formation on closed flux surfaces was found to limit \bar{n}_e by causing an H–L confinement transition; this process was usually observed when the divertor transitioned from partial to total detachment (described in Section 2). In practice, MARFEs were avoided [5] by low edge safety factor operation and divertor pumping. We found that MHD modes can be de-stabilized at densities as low as $\bar{n}_e/n_{GW} \sim 0.8$ during pellet fueling; the cause is unclear. MHD activity was observed over a wide heating power range but was avoidable at $P_{\text{heat}} < 3$ MW. By studying each process and selecting conditions to avoid it, we have achieved [4] H-mode discharges at $\bar{n}_e/n_{GW} \sim 1.5$ for up to 600 ms. These discharges were ELM-free, and owing to core impurity accumulation, ended in a central radiative collapse. Our effectiveness in heating the center was limited by the neutral beam technique; the heating deposition became hollow during the high density phase. Upcoming experiments will rely on pellet-triggered ELMs for impurity control and alternate heating techniques.

2. Partial detachment dependence on heating power

This section discusses the most common density limiting process in divertor discharges, divertor detachment, and

discusses the difference between complete and partial detachment. Complete divertor detachment is characterized [6] by a drop in the divertor D_α emission and the target plate particle flux. Usually detachment slightly precedes or is concomitant with the high density change from H-mode to L-mode confinement, which occurs close to the time that a MARFE forms on closed flux surfaces [7,8]. The first phase [9] of detachment is PDD, in which the particle flux at the strike point drops significantly but increases on the SOL side.

By itself, PDD does not cause a density limit – indeed the density can be increased by up to 10–30% beyond this point without a reduction in energy confinement. Accompanying partial detachment is the formation of a “divertor” MARFE on open field lines. Note that the PDD and divertor MARFE can be maintained in a quasi-steady manner [7]. If density is increased much beyond the PDD limit, this divertor MARFE grows/moves onto closed field lines above the X-point and H-mode confinement is lost [4,9]. Thus PDD is the first phase of a density limit process in the sense it can lead to total detachment and an H–L confinement transition. In DIII-D LSN discharges with the ion-grad-B drift toward the X-point, outboard divertor total detachment is almost always accompanied by an H–L confinement transition. Note that the inboard divertor is partially detached [10] at our normal H-mode operating density but this does not adversely impact energy confinement nor does it impose a density limit. In the remainder of this paper, all references to detachment are implicitly to partial detachment and the terms will be used interchangeably.

Models for detachment onset have predicted a strong heating power dependence of the upstream separatrix n_e and T_e just prior to detachment onset. Previous experimental studies [3,11] have shown that $\bar{n}_e \propto P_{\text{heat}}^\alpha$, where $\alpha < 0.15$. Here we examined parameters at the separatrix with our high resolution Thomson Scattering system. The discharge conditions were: $I_p = 1.0$ mA, $B_T = 2.1$ T, $q_{95} = 6.6$, $\kappa_{95} = 1.8$, $2.4 < P_{\text{NBI}} < 10$ MW. A slow density ramp was used to observe PDD onset, total detachment and the density limit. The gas-puffing rate was feedback-controlled to achieve the programmed density ramp rate, and at least two different density ramp rates were used at each heating power level. This technique resulted in an variable gas puff rate during the density ramp phase (e.g. Fig. 1(c), Fig. 2(c)).

Our first observation was that the PDD characteristics and time-scales differed as the heating power was changed. Fig. 1 shows time traces from a discharge with $P_{\text{NBI}} = 2.5$ MW. The PDD begins at $t \sim 2600$ –2610 ms, as evidenced by the drop in the ion saturation current (I_{sat}) at the Langmuir probe 1.2 cm on the private-flux region side of the strike point (Fig. 1(d)). The probe 1.5 cm on the SOL side of the strike point (Fig. 1(e)) shows a drop in I_{sat} at $t \sim 2645$ ms, and the probe farther in the

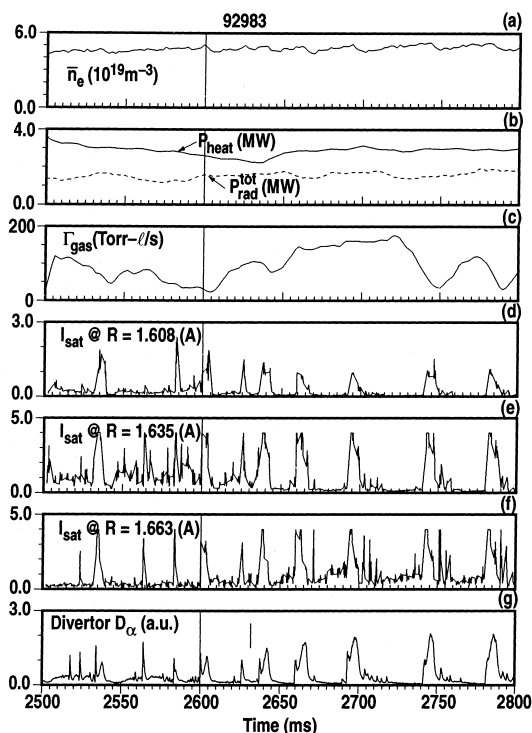


Fig. 1. Detachment characteristics for $P_{\text{NBI}} = 2.5$ MW discharge: (a) \bar{n}_e , (b) P_{heat} and total radiated power, $P_{\text{rad}}^{\text{tot}}$, (c) gas fueling rate, (d) I_{sat} from Langmuir probe 1.2 cm on private flux region side of separatrix, (e) I_{sat} from Langmuir probe 1.5 cm on SOL side of separatrix, (f) I_{sat} from Langmuir probe 4.3 cm on SOL side of separatrix, (g) divertor D_α . PDD onset is indicated by vertical line. The outer strike point was at $R = 1.62$ m at detachment.

SOL (Fig. 1(f)) shows an increase in I_{sat} at about the same time. Note however the change in the ELM character (Fig. 1(g)) – the broad ~ 10 ms D_α events starting at $t = 2600$ ms occur at a frequency ~ 40 Hz and are compound ELMs, which are transient returns to L-mode observed when the heating power is near the H–L transition power (for comparison, the $P_{\text{L-H}}$ was ~ 1.6 MW at that time). The compound ELMs re-attach the outboard divertor; between ELMs, the PDD gradually reforms as evidenced by the gradual growth of the I_{sat} between ELMs, e.g. from $t = 2670$ – 2690 ms, on the probe 4.3 cm on the SOL side of the separatrix (Fig. 1(f)).

Divertor parameters after PDD onset equilibrated more quickly at high heating power than low heating power. Fig. 2 displays the detachment characteristics of a discharge with $P_{\text{NBI}} = 10$ MW. The PDD begins at $t \sim 2800$ – 2820 ms, indicated by the drop in the ion saturation current (I_{sat}) at the Langmuir probe just at the strike point (Fig. 2(d)). The probe 5.4 cm on the SOL side of the outer strike point shows (Fig. 2(f)) a

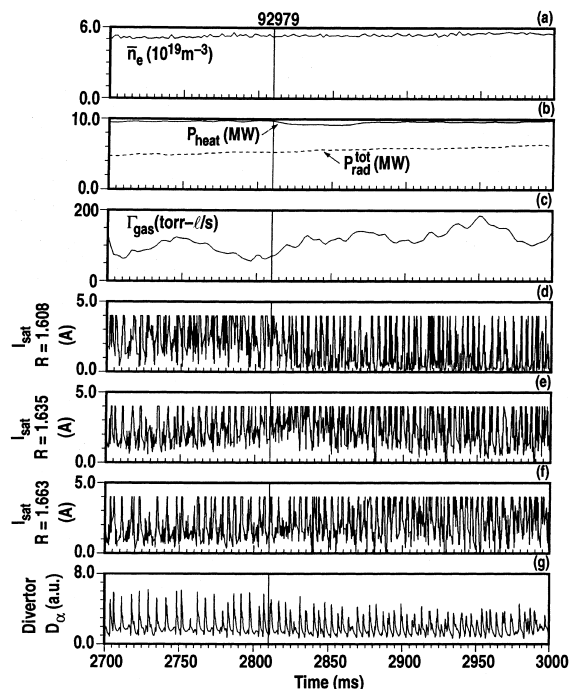


Fig. 2. Detachment characteristics for $P_{\text{NBI}} = 10$ MW discharge: (a) \bar{n}_e , (b) P_{heat} and $P_{\text{rad}}^{\text{tot}}$, (c) gas fueling rate, (d) I_{sat} from Langmuir probe at strike point, (e) I_{sat} from Langmuir probe 2.6 cm on SOL side of separatrix, (f) I_{sat} from Langmuir probe 5.4 cm on SOL side of separatrix, (g) divertor D_α . PDD onset is indicated by vertical line. The outer strike point was at $R = 1.61$ m at detachment.

marginal I_{sat} increase compared to the pre-detachment level, whereas the probe 2.6 cm on the SOL side of the separatrix shows (Fig. 2(e)) a prompt I_{sat} increase followed by a relaxation back down close to pre-detachment level. In this case the D_α trace (Fig. 2(g)) shows normal ELM events which change only modestly after PDD onset. The difference in detachment character at high and low heating power can then be attributed to the difference in the edge power flow to the $P_{\text{L-H}}$. The $P_{\text{NBI}} = 5$ MW discharges exhibit a strike point I_{sat} drop slower than the $P_{\text{NBI}} = 10$ MW case but an equilibrium is achieved, this is in contrast to the $P_{\text{NBI}} = 2.5$ MW discharges which show little sign of steady behavior between compound ELM events. In these discharges, detachment appears to progress more slowly as the power relative to $P_{\text{L-H}}$ is reduced. Previously, only very fast transitions to PDD have been reported, all at power levels well above $P_{\text{L-H}}$ [3,6,7,9]; more analysis is needed to determine if the slow detachment observed here is a general feature related to $P_{\text{NBI}}/P_{\text{L-H}}$ or a by-product of the fact that the density ramp-rate was feedback-controlled, resulting in variable gas injection rate with time.

The \bar{n}_e just at detachment is almost insensitive to the heating power, consistent with previous reports [2], but the n_e^{sep} and T_e^{sep} at detachment do vary strongly with the power flowing into the SOL. Fig. 3 shows the evolution of the separatrix parameters for discharges at $P_{\text{NBI}} = 2.5, 5.0, 10$ MW. These n_e and T_e data are taken from Thomson scattering just above the outer midplane with 6.25 ms sampling time and the mapping is done with the EFITD code. There are possible systematic errors involved with the magnetic mapping, but the data clearly show that the n_e^{sep} increases strongly with P_{NBI} outside of the statistical noise in the data.

For comparison with models of detachment, the total power flow into the divertor leg being examined, i.e. the outboard leg on DIII-D, is obtained from data by subtracting the core radiated power from the total heating power, multiplying by the outboard/total power flow ratio, and subtracting off the outer SOL radiation: $P_{\text{loss}}^{\text{out}} = \eta(P_{\text{heat}} - P_{\text{rad}}^{\text{core}}) - P_{\text{rad}}^{\text{SOL, out}}$. The quantities $P_{\text{rad}}^{\text{core}}$ and $P_{\text{rad}}^{\text{SOL, out}}$ are obtained from 2-D reconstructions of the radiated power profile, and the outboard fraction of the

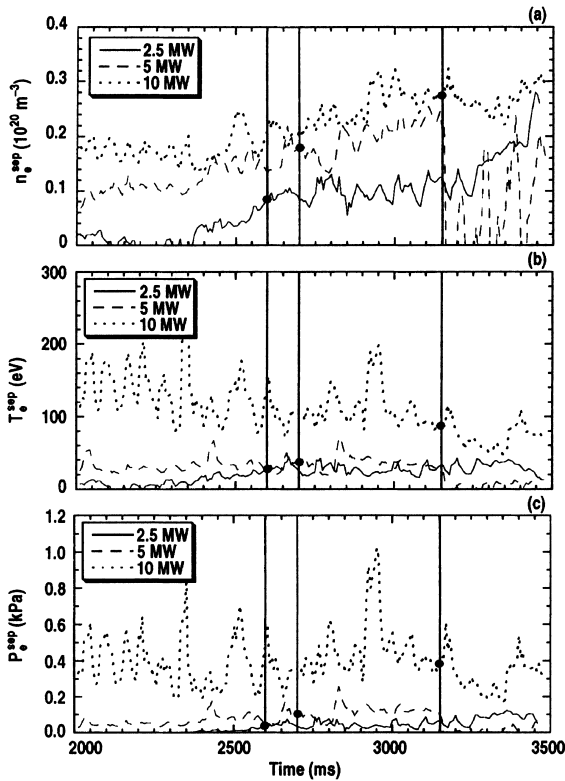


Fig. 3. Time evolution of (a) n_e^{sep} , (b) T_e^{sep} , and (c) P_e^{sep} , for discharges with P_{NBI} of 2.5, 5, and 10 MW. Detachment times are indicated by vertical lines, with the lowest power discharge detaching first and the highest power one detaching last. Note that the higher power discharges have systematically higher separatrix parameters outside of the statistical mapping errors. Dots represent values at detachment onset.

divertor power flow, η , is taken to be 0.55 as reported in previous H-mode studies [12]. Fig. 4 shows the n_e^{sep} , T_e^{sep} and P_e^{sep} at detachment as a function of $P_{\text{loss}}^{\text{out}}$. Fitted to a power dependence, n_e^{sep} scales as $\sim P_{\text{loss}}^{\text{out} 0.8}$ and T_e^{sep} scales as $\sim P_{\text{loss}}^{\text{out} 0.6}$. Also plotted in Fig. 4 are comparisons with the Borass model, discussed below.

3. Comparison of results with Borass SOL transport model

In this section we compare results of the detachment experiment with Borass' general 2-point model [13] of the SOL and divertor plasma. This model is derived from consideration of the SOL in Cartesian geometry and results in four coupled equations. Derivation of the equations is given in Ref. [13]. We reproduce the equations and necessary relations below with the explicit goal of giving the reader sufficient information to independently verify our calculations.

$$n_D = \frac{n_B T_B}{2T_D}, \quad (1)$$

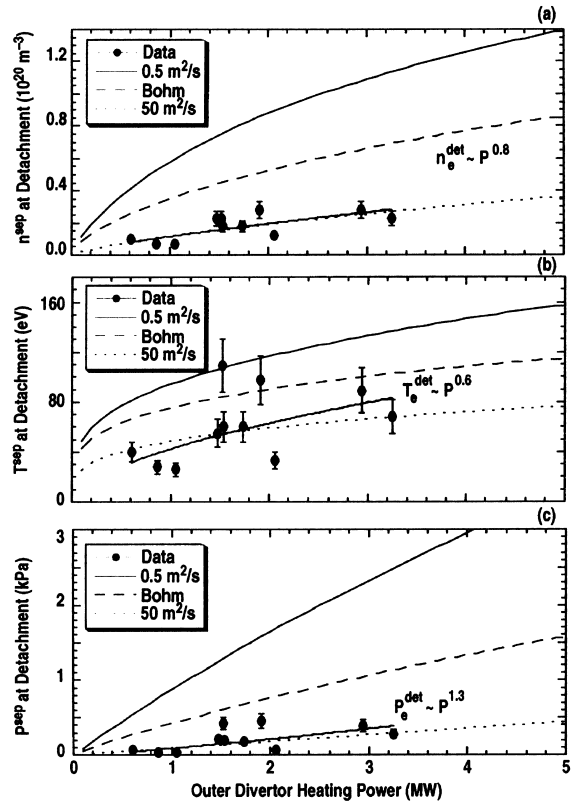


Fig. 4. Scaling for (a) n_e^{sep} , (b) T_e^{sep} , and (c) P_e^{sep} with the outer SOL loss power. Power law fits to the data are shown, as well as calculations with the Borass model with three different radial transport rates.

$$\Delta = \frac{5c}{3} \frac{\alpha_{D_B} n_B T_B^2}{2e q_{\perp} B_t}, \quad (2)$$

$$T_B = \left(\frac{49}{4\kappa} \frac{\alpha_{q_{\perp}} q_{\perp} L L_S}{\Delta} \right)^{2/7} \left[1 - \left(\frac{T_D}{T_B} \right)^{7/2} \right]^{-2/7}, \quad (3)$$

$$\frac{L_S q_{\perp}}{\Delta_E} = \zeta \beta c_s n_D + c_{\text{rad}} \gamma_{\text{imp}} n_D^2 l + \gamma T_D c_s n_D, \quad (4)$$

where n_D is the divertor density, T_D is the divertor temperature, n_B is the upstream separatrix density, T_B is the upstream separatrix temperature, Δ is the upstream SOL temperature width, α_{D_B} is the Bohm diffusion multiplier, q_{\perp} is the power flux into the outer half of the SOL, B_t is the toroidal field magnitude, $\alpha_{q_{\perp}}$ is the SOL power flow poloidal profile factor, L is the field line length from stagnation to divertor target, L_S is the field line length from stagnation to X-point, κ is the electron thermal conductivity along field lines with temperature dependence removed, Δ_E is the SOL power flux width, ζ is the electron energy loss per hydrogen neutral ionization, including radiation, β is the neutral escape probability out of divertor by pumping or CX/diffusion, c_s is the ion sound speed, c_{rad} is the temperature dependent impurity radiation emissivity, γ_{imp} is the divertor impurity fraction, l is the length of radiation/recycling zone, and γ is the sheath power transmission factor.

Eq. (1) results from momentum balance, Eq. (2) from radial transport considerations, and Eq. (3) from the classical electron conduction equation. The first term on the RHS of the divertor power balance, Eq. (4) is the total energy, radiative and kinetic, lost by the electrons in ionizing the deuterium atomic recycling flux. The second term on the righthand side of Eq. (4) is the impurity radiation loss, and the third term is the power flux transmitted through the sheath to the target. We use the same formulation for the recycling probability, β , as given in Ref. [13]. The other relationships needed to solve the above equations are:

$$q_{\perp} = \frac{P_{\text{loss}}^{\text{out}}}{A_{\text{SOL}}^{\text{outer}}} \cong \frac{P_{\text{loss}}^{\text{out}}}{2\pi^2 R a \sqrt{K}}, \quad (5)$$

$$\kappa = 3.16 \frac{3}{4\sqrt{2}\pi} \frac{1}{m_e^{1/2} e^4 \ln \Lambda}, \quad (6)$$

$$L_S \cong \pi(R + a/2) * q_{95}, \quad (7)$$

$$L \cong L_S + \frac{\sqrt{2} H_x}{(a^* \sqrt{1 + K^2})} * q_{95} * (R + a/2), \quad (8)$$

$$\zeta \cong 17.5 + (5.0 + 37.5/T_D) * \log(1e15/n_D);$$

$$\xi, T_D \text{ in eV}; \quad (9)$$

$$c_s = \sqrt{\frac{2k_B T_D}{m_i}}, \quad (10)$$

$$l \cong \sqrt{2} H_x, \quad (11)$$

where $P_{\text{loss}}^{\text{out}}$ is the total power flow into outer half of the SOL, η is the ratio of outer leg power to total heating power, a is the plasma minor radius, R is the plasma major radius, K is the plasma elongation, q_{95} is the edge safety factor, m_e is the electron mass, m_i is the deuteron mass, e is the electron elementary charge, $\ln \Lambda$ is the Coulomb logarithm, H_x is the X-point height off the floor, and k_B is the conversion factor from eV to J.

The equations set was solved for $P_{\text{loss}}^{\text{out}}$ between 0.1 and 5 MW and the model calculations for three different radial transport rates are compared with data in Fig. 4; good agreement of the detachment n_e^{sep} dependence on $P_{\text{loss}}^{\text{out}}$ is obtained. We assumed detachment onset occurred at $T_D = 5$ eV in the model. The following additional inputs were used: $\alpha_{D_B} = 1$, $\alpha_{q_{\perp}} = 1$, $c_{\text{rad}} = 3 \times 10^{-18}$ W m³/s (carbon at 5 eV), $\gamma_{\text{imp}} = 0.02$ (carbon). The other geometric parameters were given earlier. In Fig. 4, the Bohm radial transport coefficient varies as T_e/B_T and ranges from 1.2 to 3.5 m²/s for T_B from 40 to 120 eV. The other two curves in Fig. 4 assume a fixed radial transport coefficients, in which case Eq. (2) was re-derived and Eqs. (1)–(4) were solved without the assumption of Bohm transport. The $D_{\perp} = 0.5$ m²/s corresponds to a typical value obtained from data-constrained 2-D modeling of DIII-D H-mode data, and the $D_{\perp} = 50$ m²/s was used to determine the level of transport needed to make the model calculations come into quantitative agreement with the data. Thus, the model produces very close to the same scaling for n_e^{sep} at detachment (data $n_e^{\text{sep}} \sim P_{\text{loss}}^{\text{out}0.8}$, model $n_e^{\text{sep}} \sim P_{\text{loss}}^{\text{out}0.7}$) as compared with data, but the absolute magnitudes can only be obtained with very high radial transport rates. However the dependence of T_e^{sep} at detachment is more than $2 \times$ stronger than predicted by the model (data $T_e^{\text{sep}} \sim P_{\text{loss}}^{\text{out}0.6}$ model $T_e^{\text{sep}} \sim P_{\text{loss}}^{\text{out}0.3}$).

The difference between the model and data cannot be explained solely by a possible systematic error in the mapping of the separatrix location. Fig. 4(b) shows that the highest experimental T_e^{sep} at detachment is ~ 100 eV. Movement of the separatrix radially inward to obtain a quantitative match of the experimental n_e^{sep} with the model calculation for either the Bohm or 0.5 m²/s radial transport coefficients would imply that the SOL temperature at detachment would increase to >150 – 200 eV at the highest heating power. This would imply a parallel temperature gradient which cannot be sustained for the connection length of DIII-D. Nevertheless, it is noteworthy that the maximum n_e^{sep} shown in Fig. 3 at any time was 3×10^{19} m⁻³, significantly lower than the $n_e^{\text{sep}} \sim 7 \times 10^{19}$ m⁻³ reported [7] by ASDEX-Upgrade at the L-mode density limit. This significant difference between comparable tokamaks merits investigation.

4. Discussion and conclusions

We have shown [4] that different processes can limit the density in H-mode plasmas under different conditions. By tailoring conditions to avoid these processes, H-mode discharges with $\bar{n}_e/n_{GW} \leq 1.5$ have been achieved for up to 600 ms. Use of pellets to trigger ELMs could have prevented the impurity accumulation and radiative collapse; upcoming experiments will focus on this as well as fueling from the high-field side. We have also derived [5] a scaling for an edge density limit based on MARFE formation and the empirically determined energy confinement scaling law; this density limit is almost identical to Greenwald scaling and it suggests that the key to avoiding this MARFE limit is by maintaining a high edge/pedestal T_e .

We have observed that the character of the detached plasma state varies with the heating power level. Specifically the divertor plasma approaches a quasi-steady equilibrium more quickly at higher heating power. We found that the n_e^{sep} and T_e^{sep} at detachment onset increase strongly with the applied heating power. The n_e^{sep} dependence is in contrast to the global \bar{n}_e at detachment, which is relatively insensitive to the heating power. This apparent difference is explained by the observation that gas puffing preferentially increases the edge/SOL density relative to the central density. We find that the empirical power law dependence of the $n_e^{\text{sep}} \sim P_{\text{loss}}^{\text{out}0.8}$ is reasonably close to the dependence predicted from the Borass SOL transport model ($n_e^{\text{sep}} \sim P_{\text{loss}}^{\text{out}0.7}$), although the absolute magnitude of the model n_e^{sep} is comparable only at extremely high radial transport rates. Thus, it is clear that the core density is not the limiting factor in PDD. Since PDD by itself is not a density limiting mechanism, this separability would be crucial in tailoring a favorable density profile in the core for fusion reactions while

staying just above the detachment limit in the SOL for heat flux reduction.

Acknowledgements

Work supported by the US Department of Energy under Contract Nos. DE-AC03-89ER51114, DE-AC05-96OR22464, DE-AC04-94AL85000, and Grant No. DE-FG03-95ER54294. We thank the DIII-D Operations staff and Boundary Physics groups.

References

- [1] M. Greenwald et al., Nucl. Fusion 28 (1988) 2199.
- [2] T.W. Petrie et al., Nucl. Fusion 33 (1993) 929.
- [3] F.W. Perkins et al., Proceedings of the 16th International Fusion Energy Conference, 7–11 October 1996, Montreal, Canada, paper F1-CN-64/FP-24.
- [4] R. Maingi et al., Phys. Plasmas 4 (1997) 1752.
- [5] M.A. Mahdavi et al., Recent H-mode density limit experiments on DIII-D, presented at 24th European Conference on Controlled Fusion and Plasma Physics, 9–14 June 1997, Berchtesgaden, Germany, Phys. Rev. Lett., to be submitted.
- [6] T.W. Petrie et al., J. Nucl. Mater. 196–198 (1992) 848.
- [7] T.W. Petrie et al., J. Nucl. Mater. 241–243 (1997) 639.
- [8] V. Mertens et al., Proceedings of the 16th International Fusion Energy Conference, 7–11 October 1996, Montreal, Canada, paper F1-CN-64/A4-4.
- [9] T.W. Petrie et al., Nucl. Fusion 37 (1997) 321.
- [10] R. Maingi et al., J. Nucl. Mater. 220–222 (1995) 320.
- [11] T.W. Petrie et al., these Proceedings.
- [12] A.W. Leonard et al., J. Nucl. Mater. 220–222 (1995) 325.
- [13] K. Borass, Nucl. Fusion 31 (1991) 1035.